Invited Paper

Multifunctional III-nitride dilute magnetic semiconductor epilayers and nanostructures as a future platform for spintronic devices

Matthew H. Kane[a,b], Martin Strassburg[a,d], Ali Asghar[a], Qing Song[c], Shalini Gupta[a], Jayantha Senawiratne[d], Christoph Hums[d,e], Ute Haboeck[e], Axel Hoffmann[e], Dmitry Azamat[e], Wolfgang Gehlhoff[e], Nikolaus Dietz[d], Z. John Zhang[c], Christopher J. Summers[b], Ian T. Ferguson[a,b,*]

[a]Georgia Institute of Technology, School of Electrical and Computer Engineering, Atlanta, GA, USA 30332-0250;
[b]Georgia Institute of Technology, School of Materials Science and Engineering, Atlanta, GA, USA 30332-0245
[c]Georgia Institute of Technology, School of Chemistry and Biochemistry, Atlanta, GA, USA 30332-0400;
[d]Georgia State University, Department of Physics and Astronomy, Atlanta, GA, USA 30303;
[e]Institut für Festkörperphysik, Technische Universität Berlin, D - 10623 Berlin, Germany

ABSTRACT

This work focuses on the development of materials and growth techniques suitable for future spintronic device applications. Metal-organic chemical vapor deposition (MOCVD) was used to grow high-quality epitaxial films of varying thickness and manganese doping levels by introducing bis-cyclopentadienyl as the manganese source. High-resolution X-ray diffraction indicates that no macroscopic second phases are formed during growth, and Mn containing films are similar in crystalline quality to undoped films Atomic force microscopy revealed a 2-dimensional MOCVD step-flow growth pattern in the Mn-incorporated samples. The mean surface roughnesses of optimally grown $Ga_{1-x}Mn_xN$ films were almost identical to that from the as-grown template layers, with no change in growth mechanism or morphology. Various annealing steps were applied to some of the samples to reduce compensating defects and to investigate the effects of post processing on the structural, magnetic and opto-electronic properties. SQUID measurements showed an apparent ferromagnetic hysteresis behavior which persisted to room temperature. An optical absorption band around 1.5 eV was observed via transmission studies. This band is assigned to the internal Mn^{3+} transition between the ^5E and the partially filled $^5T_2$ levels of the ^5D state. The broadening of the absorption band is introduced by the high Mn concentration. Recharging of the Mn^{3+} to Mn^{2+} was found to effectively suppress these transitions resulting in a reduction of the magnetization. The structural quality, and the presence of Mn^{2+} ions were confirmed by EPR spectroscopy, meanwhile no Mn-Mn interactions indicative of clustering were observed. The absence of doping-induced strain in $Ga_{1-x}Mn_xN$ was observed by Raman spectroscopy.

Keywords: Spintronics diluted magnetic semiconductor, GaMnN, ferromagnetic semiconductor, MOCVD

1. INTRODUCTION

1.1. Applications of diluted magnetic semiconductors nanostructures

The use of the spin property of the electronic represents a new field known as 'spintronics' [1-4]. The use of the spin property of an electron as a carrier of electronic information is a distinct paradigm shift from traditional electronic devices. Two fundamental characteristics make electron spin an interesting property: the non-volatile nature of spin

*Corresponding Author: ianf@ece.gatech.edu

Quantum Sensing and Nanophotonic Devices II, edited by Manijeh Razeghi, Gail J. Brown, Proceedings of SPIE Vol. 5732 (SPIE, Bellingham, WA, 2005)
0277-786X/05/$15 · doi: 10.1117/12.582980

makes it useful for memory applications, while the inherently quantum nature of electron spin means it may be suitable for quantum computation. The addition of the spin degree of freedom to traditional devices could also benefit optoelectronics. Through the use of optical domain polarization, up-conversion and down-conversion of the light source through spin-based emitters and detectors can provide an interface that leads to enhanced functionality in traditional semiconductor optoelectronic devices. In addition, many of the systems proposed for spintronics exhibit large magneto-optical effects which could be used for integrated magneto-optic structure and nonvolatile optical memories.

Diluted magnetic semiconductors (DMS) are attractive materials candidates for spintronics, as they can have the inherent properties of both semiconductor and ferromagnetic materials. These systems consist of a traditional III-V, II-VI, or group IV semiconductor into which a small fraction of a magnetic element, such as interior transition metal like Mn, has been introduced. These DMS materials can exhibit ferromagnetic behavior under certain doping and processing conditions. These ferromagnetic materials could provide a stable source of spin polarized carriers, which combined with the ease of integration into existing semiconductor technology, may enable future spintronic devices in these DMS systems.

1.2. Theories of ferromagnetism in III-Nitride magnetic semiconductors

Traditional III-V DMS, such as $Ga_{1-x}Mn_xAs$, are well-established, though the Curie temperatures of these materials are limited to only around 170K [5]. The ferromagnetic ordering is though to originate from a long range coupling of the magnetic centers through the free hole carriers [6]. When applying this mean field model to the GaN system, the Curie temperature is predicted to be above room temperature, though this model requires larger substitutional Mn concentrations (~5%) and hole concentrations ($1x10^{20}$) than may be possible to achieve in the $Ga_{1-x}Mn_xN$ system. Other models have been develops based on first principles density functional theory calculations using the local spin density approximation that also predict ferromagnetism in the nitride compounds [7-9]. In these models, the Mn 3d levels do not overlap and are not strongly hybridized with the GaN s,p levels as is seen in $Ga_{1-x}Mn_xAs$; nevertheless, ferromagnetism is expected in this system. Other theoretical predictions suggest that a Mn-induced impurity band provides a mechanism for effective-mass transport that can be exploited for carrier mediation [7, 10]. Sato et al. [8] showed that the incorporation of Mn facilitates the formation of a sharp ^5E impurity band and a broader $^5T_2$ impurity band altering the electronic structure in the bandgap of $Ga_{1-x}Mn_xN$. The broadening in the partially filled $^5T_2$ band stabilizes the ferromagnetism via the double exchange interaction [8, 11] provided the Fermi level is in this defect band.

1.3. Obstacles to ferromagnetic applications of GaMnN

Experimental efforts have successfully grown $Ga_{1-x}Mn_xN$ which has exhibited room temperature ferromagnetism by a number of different means, including bulk crystal growth [12-14], ion implantation [15-21], post-growth diffusion [22], and molecular-beam epitaxy [23-26]. It is unclear at this point whether the ferromagnetic behavior is due to the homogeneous behavior of the alloy, or rather due to ferromagnetic nanoclusters. All of the ferromagnetic material grown at this time is either insulating or n-type, which is inconsistent with the prevailing theory requiring a spin polarized hole gas to mediate ferromagnetism. In addition, the bulk crystallites grown by the ammonothermal method exhibited paramagnetic behavior. Additionally, the Curie temperature reported for MBE grown $Ga_{1-x}Mn_xN$ has varied widely from 15K to 940K. Nanoscale clusters have been observed in some samples by transmission electron microscopy [27], though only at extremely high doping levels (>8%) and it has not been shown conclusively that this behavior will be the same at lower concentrations. MBE grown $Ga_{1-x}Mn_xN$ has not exhibited a magnetic circular dichroism signal consistent with a spin-split density of states at the valence band typical of other ferromagnetic DMS compounds [28]. Recently, a close correlation between transition metal occupancy on the Ga site and magnetic behavior has been demonstrated in the GaCrN system [29]. Other work has provided evidence of a correlation between Curie temperature increase and Mn doping level in GaMnN [30], though the variation in Curie temperature is within the range of Ga/Mn stoichimetric variations in the ferrimagnetic metallic perovskite $Mn_{4-x}Ga_xN_{1-y}$, which may by the leading impurity phase in GaMnN-based materials [24]. Thus, further work is needed prior to the integration of these materials into room temperature spintronic devices.

Because these compounds are inherently non-equilibrium, it is imperative to understand both the non-equilibrium growth processes involved as well as the effects of any post-growth processing on these material systems. For example, $Ga_{1-x}Mn_xAs$ is grown almost exclusively by low temperature molecular beam epitaxy [5, 31], and during growth and annealing there is always a competition between the dilute $Ga_{1-x}Mn_xAs$ phase and the MnAs second phase.

Careful low temperature annealing can result in improved magnetic behavior due to the reduction of Mn interstials [32], but at elevated temperatures can result in second phase segregation [33]. The growth and annealing effects in $Ga_{1-x}Mn_xN$ are less well established. As many of the initial results for $Ga_{1-x}Mn_xN$ were of implanted material, there would always be some post processing required from this technique. Excessive annealing was also found to produce second phases in as-grown and implanted material, though the exact phase produced varied from Mn_3N_2 and $Mn_6N_{2.58}$ [34] to GaMn intermetallics [35] to Mn_3GaN [16, 24] depending on the processing conditions. Ultimately, the optimal growth and processing path for room temperature ferromagnetic $Ga_{1-x}Mn_xN$ must be understood for future applications.

1.4. Use of nanostructures for spintronics

Nanostructures have been shown to enhance the performance and efficiency of optoelectronic devices. The behavior of carriers in nanostructures may also allow for the enhancement of the ferromagnetic semiconductor behavior. Quantum confinement within quantum wells allows for splitting of the heavy hole-light hole spin degeneracy and an increase in the overall spin polarized recombination efficiency [36]. Quantum dots are also thought to be a method for achieving quantum computation within the solid state [37]. In addition, quantum confinement may lead to an enhancement of the Curie temperature as has been reported for InMnAs [38]. Quantum confined structures are also expected to have longer coherence times than in the bulk, which may provide a pathway for increasing the spin lifetime in nitride-based ferromagnetic semiconductor devices for practical applications. Because the growth constraints for 3-dimensional nanostructures within the nitride system are so tight, it may not be possible to find conditions which will support both the dilute magnetic semiconductor behavior and necessary size restrictions for quantum confinement. Another obstacle to overcome will be that growth procedures which promote small island agglomeration may also lead to magnetic atom clustering, which may not be practical for certain devices.

1.5. Overview

$Ga_{1-x}Mn_xN$ epilayers and nanostructures have been grown via MOCVD. The as-grown films are specular and have a reddish tinge indicative of substitutional Mn incorporation with excellent single phase crystalline quality. SIMS confirmed homogeneous Mn incorporation and no second phases (e.g., Mn_xN_y) were observed in XRD. Annealing in a non-reactive atmosphere resulted in surface decomposition of the films. All the GaMnN samples showed room temperature magnetism except for the highest Si concentrations $> 10^{19}$ cm^{-3}. In this work, the experimental identification of the Mn ion charge state and the presence of bands in the bandgap of GaN is investigated by optical spectroscopy and electron spin paramagnetic resonance (EPR) [9, 10, 39, 40]. Photoluminescence emission bands in the blue (~3 eV) have been observed in MOCVD-grown and Mn-implanted GaN:Mn [21, 41-44]. This provides information on defects and disorder induced by the Mn incorporation in GaN. Additional information about the position of the Fermi-level and the existence of an impurity band was obtained using absorption spectroscopy revealing energy states around 1.1 eV, 1.5 eV and 1.8 eV. These states were assigned to interatomic transitions or to transitions between the Mn-states and the valence band, or to both [10, 40, 41].

In this paper, an investigation of the Fermi level dependence of the optical and structural properties of $Ga_{1-x}Mn_xN$ with room temperature magnetization behavior is presented. MOCVD growth was applied in order to increase the concentration of Mn incorporated on Ga sites in the desired charge state (Mn^{2+}) to support the ferromagnetism while maintaining the diluted magnetic semiconductor properties. Broadening of the $^5T_2$ state according to the high Mn concentration was confirmed by a broad absorption band detected around 1.5 eV. Its linewidth and magnitude scaled with the Mn concentration, and showed a strong dependence on the position of the Fermi-level that was in addition varied by silicon co-doping and/or annealing. No strain and no significant concentration of free carriers were introduced by Mn alloying as confirmed by Raman spectroscopy. This was consistent with electrical measurements that showed the as grown material to highly resistive. These results suggest that a double exchange interaction is the most likely mechanism for ferromagnetism in $Ga_{1-x}Mn_xN$.

2. Methodology

2.1. Growth procedure

$Ga_{1-x}Mn_xN$ films with Mn concentration up to ~2% were grown in an Emcore MOCVD D-125 rotating disk reactor with a short jar configuration. The reactor has a specially modified flow flange injection system which has been modified with dual injector blocks to minimize prereactions of the gallium and manganese precursors in the transport phase. Mn concentration in the film was varied up to ~2% by controlling the molar flow ratios of the cursors. All films were grown at standard GaN growth temperatures on 2" sapphire substrates. Initially, two micron thick GaN buffer layer templates were grown using standard GaN techniques on c-sapphire. Ammonia, trimethyl gallium (TMG) and bis-cyclopentadienyl manganese (Cp_2Mn), bis-cyclopentadienyl magnesium (Cp_2Mg) and silane (SiH_4) were used as the nitrogen, gallium, manganese, p-, and n-dopant sources respectively for $Ga_{1-x}Mn_xN$. A 30nm GaN capping layer was deposited on top of some samples in order to provide a non-manganese terminated surface. Some samples were subsequently annealed face-down on GaN templates in flowing nitrogen ambient at temperatures ranging from 700°C to 900°C.

2.2. Characterization

Detailed characterization of these films was performed, including X-ray diffraction (XRD), secondary ion mass spectroscopy (SIMS), atomic force microscopy (AFM), superconducting quantum interference device magnetometry (SQUID), and electrical transport measurements. Crystalline quality and phase purity were determined by high-resolution XRD using a Philips X'Pert Pro MRD diffractometer. Atomic force microscopy (AFM) was performed using a PSIA XE-100. Magnetic properties were analyzed using a Quantum Design MPMS 5S SQUID magnetometer at temperatures from 5 to 300 K. Secondary Ion Mass Spectroscopy (SIMS) depth profiles were performed on the samples using an Atomika Instruments Ionmicroprobe A-DIDA 3000. Photoluminescence (PL) data was obtained using a frequency-doubled Titanium-Sapphire laser and transmission measurements were performed using the red and infrared spectrum of a halogen lamp. The emitted and transmitted light was detected by a photomultiplier attached to a 0.24 m monochromator with a spectral resolution of better than 1 nm for emission and better than 6 nm for transmission experiments which is adequate for the broad band transitions investigated in this work.

3. Results and discussion

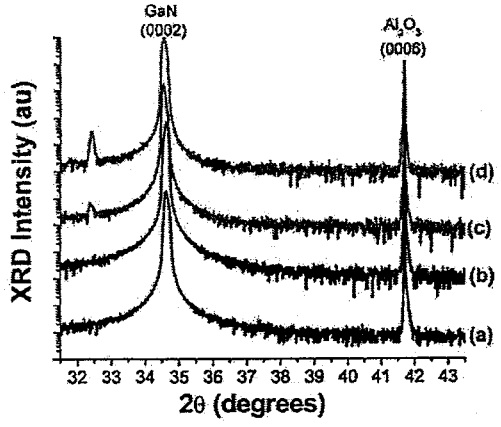

Figure 1. XRD diffraction scans of (a) undoped GaN template layer, (b) as-grown MOCVD GaMnN layers, (c) MOCVD grown GaMnN layer annealed at 700°C, and (d) MOCVD grown GaMnN layer annealed at 900°C

3.1. High Resolution X-Ray Diffraction

The as-grown films are specular and increased in reddish tint with increasing thickness. Varying the temperature outside the optimal growth band resulted in the appearance of hexagonal GaN growth temperature defects which were visible via optical microscopy, or the loss of film integrity. Secondary ion mass spectroscopy (SIMS) verified the uniform incorporation of manganese within the layers. High resolution x-ray diffraction (HRXRD) was performed in order to examine the phase purity and crystalline quality of the as-grown films. In the x-ray diffraction scans, no second phases were observed in the as-grown scans, as seen in Figure 1. The peak position of the $Ga_{1-x}Mn_xN$ peaks did not shift relative to the GaN peaks at the low doping levels, indicating a lattice parameter similar to that of GaN, though this may be influenced by the underlying template layers in some of the films. The linewidth of the scans were within few houndred arcsec, showing no significant increase compared to width of the template: Rocking curve widths for the (0002) and (10-

12) reflections in samples doped at ~1% Mn were 150 and 522 arcsec, compared with 179 and 518 arcsec for the underlying template layer. Upon annealing at temperatures as low as 700°C, other phases do appear in the ω–2θ scans. These most closely index to the (110) reflections of the Mn_3GaN phase. This phase has been observed previously as noted above though this peak is quite close to a GaMn intermetallic phase which has been reported to be present [35]. This second phase is not observed in the samples capped with a thin GaN layer, even at annealing temperatures of 900°C, though further investigations are required to determine the post-annealing phase purity of the capped samples. The $Mn_6N_{2.58}$ and Mn_3N_2 phases were not observed via XRD in the annealed MOCVD grown samples as has been previously reported in implanted samples [16].

3.2. Atomic Force Microscopy

Additional information about the growth mechanism and annealing effects is derived from studies of the atomic force microscopy images of the $Ga_{1-x}Mn_xN$ layers. Figure 2 shows images of the as-grown layers and layers annealed under various temperatures. The overall film quality is smooth with atomic layer surface steps visible. The root mean square (RMS) surface roughnesses are between 4 and 11 Å depending on the film and underlying template layer. Clear step flow growth patterns are seen in the as-grown MOCVD sample scans, which are typical of two-dimensional growth modes seen in GaN MOCVD; this mode does not change with the introduction of Mn into the growth process. Films grown outside the optimal temperature bands exhibit hexagonal GaN temperature defects, which can be seen in both the AFM as well as via optical microscopy. The RMS roughnesses of the Mn incorporated film is similar to that of the underlying template layer (3.8 Å vs 3.4 Å). With low temperature annealing (700°C), there is little change in the morphology of the layer. With annealing at higher temperatures, however, there is a significant difference in the AFM images. The 900°C AFM image of the uncapped sample shows clear spots of what is likely second phase precipitate on the surface. Close inspection of the 800°C image shows smaller spots of these second phases which are likely at nucleation sites. On the other hand, the annealed capped samples show no change in surface morphology even at the elevated temperature. This suggests that the primary mechanism for the decay of the thermodynamically unstable $Ga_{1-x}Mn_xN$ compound is through nitrogen desorption and phase rearrangement of the surface at the $Ga_{1-x}Mn_xN$-to-atmosphere interface in the absence of a reactive nitrogen environment that is present during MBE or MOCVD growth.

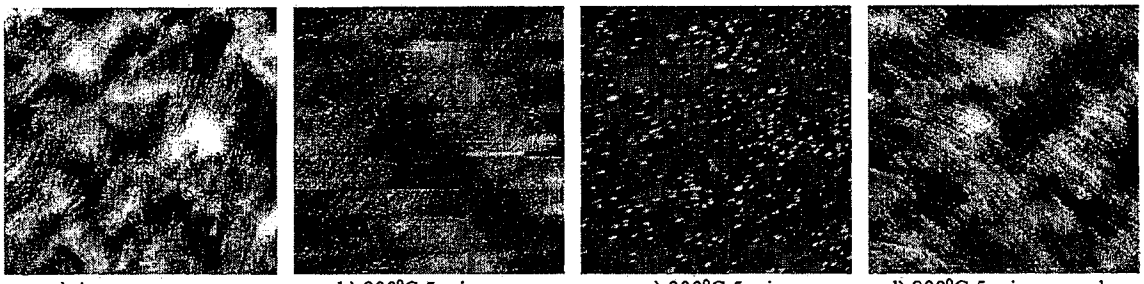

a) As grown b) 800°C 5 min c) 900°C 5 min d) 800°C 5 min, capped

Figure 2: Atomic force microscopy images from the $Ga_{1-x}Mn_xN$ (x=0.015) terminated (a-c) and GaN terminated (d) MOCVD grown $Ga_{1-x}Mn_xN$ samples under various annealing conditions. All scans are 10 μm x 10 μm. RMS roughness values from left to right are: top row: 5.68 Å, , 5.94 Å, 7.71 Å, and 6.88 Å,

3.3. Magnetic property measurements

SQUID magnetometry was performed to determine the overall magnetic behavior of the MOCVD grown $Ga_{1-x}Mn_xN$ films. Ferromagnetic hysteresis was observed in the as-grown $Ga_{1-x}Mn_xN$ films. No evidence of second phases or superparamagnetic clusters was observed in the magnetic property data. Figure 3 shows representative magnetization behavior of these samples. The curves are shown at 300 K, and in general there is little deviation for these curves at 5 K, indicating the hysteresis is due to a phase with a high Curie temperature (T_C>400 K). The saturation magnetization of the as-grown $Ga_{1-x}Mn_xN$ samples with x=0.02 is 11.6 emu/cm^3, which based on the expected doping levels associated with the precursor molar flows corresponds to a magnetic moment of 2.4 μ_B/Mn. Upon annealing, this magnetization of the sample drops precipitously, as seen in figure 3. There is still some area remaining in the hysteresis loop observed in this sample, indicating that ferromagnetic phase is not completely lost or their may be a small contribution from ferromagnetic second phases or local areas of the alloy which were unaffected by the anneal. A close inspection of the zero-field cooled versus field-curves temperature dependent magnetization curves indeed shows a small irreversibility which would suggest a minor contribution from ferromagnetic phase precipitates. A similar behavior is seen in the MOCVD-grown samples co-doped with silicon, where prior to co-doping, a large magnetic moment per atom can be seen. The magnetic moment decreases with increasing Si doping concentration and is nearly destroyed upon a target doping concentration of 10^{20}/cm^3 Si.

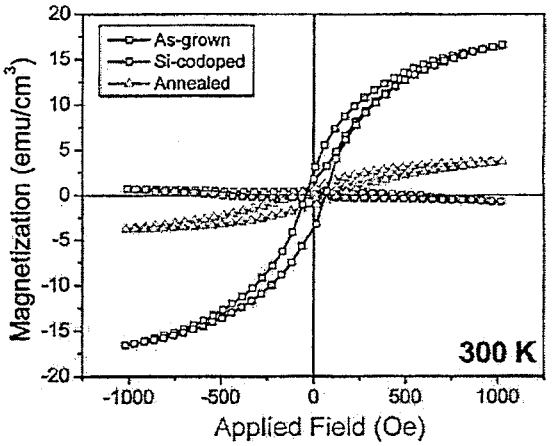

Figure 3: Magnetization vs applied field taken at room temperature for as-grown $Ga_{1-x}Mn_xN$ (x=0.01), and samples following 800°C anneal and codoping with high levels of silicon (~1e20). Note the decreased magnetic signature with annealing or silicon codoping

The large decrease in the magnetization with co-doping and annealing suggests a common origin to the deterioration of the magnetic properties of $Ga_{1-x}Mn_xN$ with either doping or annealing. Recalling the double exchange model of ferromagnetism in the DMS described above, this can be understood. In order to be able to support ferromagnetism, the Fermi level of the system must be in the spin split DOS Mn-impurity band, which is essentially midgap. The Fermi level must lie below the $Mn^{2+/3+}$ acceptor level so that the t_2 band is only partially filled and can support hopping and double exchange that stabilizes the ferromagnetism. Increasing the Fermi level by introducing donor states above this level results in trapping of donor electrons filling the t_2 band and a conversion from the Mn^{3+} (d^4) to the Mn^{2+} (d^5) configuration, thus eliminating the hopping pathway necessary for ferromagnetic ordering. These donor states may be introduced by either intentional co-doping, in the case of silicon co-doping, or by the introduction of vacancies and other shallow donor defects during the annealing process. Data reported elsewhere [45] for these same samples showed a close correlation between the optical properties and electron paramagnetic spectrum with the valence state variation and magnetic properties in this system.

3.4. Optical properties

Optical and structural measurements have been used to investigate the origin of the room temperature (RT) ferromagnetism (FM) observed in GaMnN epilayers. A detailed description of the magnetization behavior is given elsewhere but will referenced as needed [46-48]. In general, RT ferromagnetism scaled with the Mn concentration. RT FM was also observed, but significantly weaker, in MOCVD-grown semi-isolating and n-type epilayers. As described above, FM could be completely suppressed when co-doping with > $10^{19\text{-}20}$ cm^{-3} silicon atoms. This indicates that the RT FM is very sensitive to the position of the Fermi level in order that the Mn ion is in the Mn^{3+} state; however, the magnetization data alone do not provide enough information to reveal the actual origin of the RT ferromagnetism.

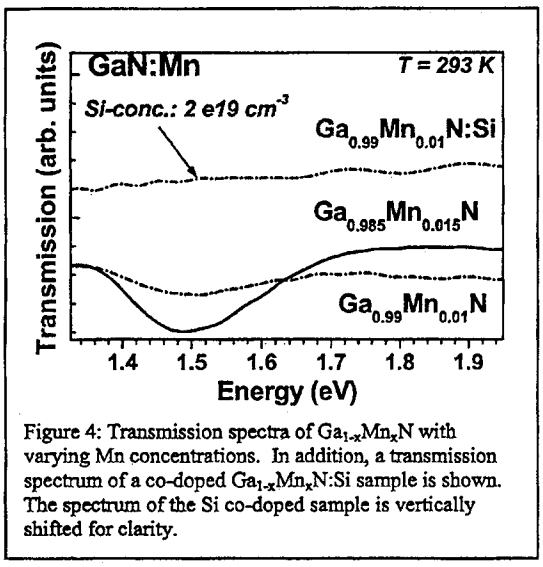

Figure 4: Transmission spectra of $Ga_{1-x}Mn_xN$ with varying Mn concentrations. In addition, a transmission spectrum of a co-doped $Ga_{1-x}Mn_xN$:Si sample is shown. The spectrum of the Si co-doped sample is vertically shifted for clarity.

In order to reveal the charge state of the incorporated Mn ions incorporated in GaN, both transmission and emission studies were performed. The transmission spectra of two samples differing in their Mn content are shown in Figure 4. The incorporation of Mn into GaN layers during MOCVD growth leads to a broad absorption band (dip in transition spectra) and a spectrally diffuse line around 1.5 eV with a larger linewidth (full width at half of maximum – FWHM) as it was observed in MBE-grown and implanted GaMnN epilayers [10, 41]. The relatively large FWHM of ~150 meV for this absorption band and an increase of its FWHM and intensity with increasing Mn concentration were observed. Mn^{3+} transitions from the E state to the partially filled T_2 levels of the ^5D state are assigned to the observed absorption band and broadened due to the high Mn concentration [8]. The transmission of the third sample, shown in Figure 4, was prepared to exhibit n-type behavior by co-doping with silicon during growth. Hall measurements showed a slight increase in the free electron density in the conduction band (at RT). This behavior is attributed to the (over-) compensation of Mn acceptor states due to the trapping of the Si donor electrons. The absence of the absorption band around 1.5 eV in the $Ga_{1-x}Mn_xN$ layer co-doped with silicon points towards its sensitivity to the position of the Fermi level. The Fermi level is shifted towards the conduction band because electrons are present at deep defects. No other absorption features were detected further in the infrared spectral range (down to 0.5 eV). This suggests that the location of the Fermi level in the investigated samples in the broad absorption band is around 1.8 eV above the valence band energy, and even closer to the conduction band than for the Si co-doped sample. However, an unambiguous proof that this Mn-induced band is the magnetism for RT FM is still needed and could be addressed by spin-sensitive spectroscopic techniques.

PL studies were performed in the UV and visible spectral range in order to further understand the ferromagnetic nature and Mn-induced midgap states of MOCVD-grown $Ga_{1-x}Mn_xN$ epilayers. The RT PL of various samples is shown in Figure 5: three as-grown samples differing in Mn concentration and one annealed sample with a Mn concentration of 1%. The blue emission band was found to govern the PL spectrum of the samples with a Mn concentration >0.5 % resulting in two distinct peaks at 3.0 eV and 2.8 eV. The band at 3.0 eV is attributed to Mn-related or Mn-induced transitions for heavily Mn doped samples. Recently, the blue band emission was observed in MBE-grown GaMnN [49], and the appearance of these bands was assigned to transitions from conduction band electrons to Mn - related states and from shallow donor (e.g., N vacancy) to Mn acceptor states [42-44, 50]. In comparison, almost no blue band emission but a pronounced yellow band attributed to intrinsic gallium defects was observed in the lightly doped GaMnN samples (<0.5%) [49], the annealed sample and the sample co-doped with Si. In the first case, the behavior is assigned to the lower amount of Mn ion available to substitute on lattice site reducing the amount of Ga vacancies. In the latter two cases, intrinsic and extrinsic shallow donor states are introduced leading to a recharging of the Mn^{3+} acceptors. This is in agreement with the reduced intensity of the absorption band around 1.5 eV that was found to decrease also by decreasing the Mn concentration and as a result of annealing. An even stronger compensation of Mn acceptors is seen for Si co-doping. The

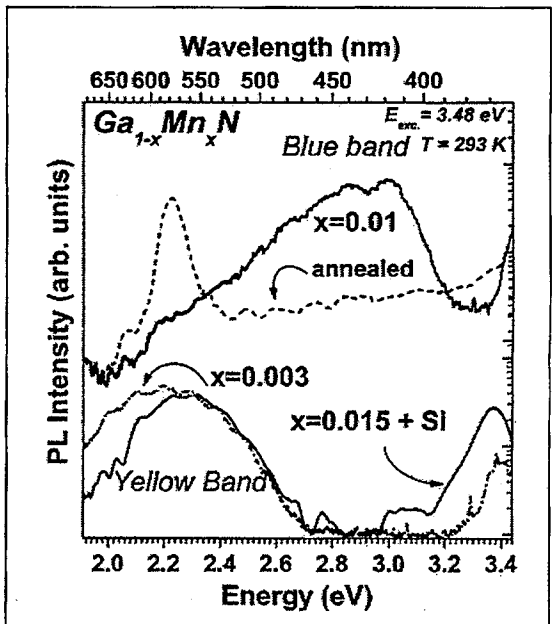

Figure 5: Photoluminescence spectra of $Ga_{1-x}Mn_xN$ recorded in the visible and UV spectral range.

PL is similar to that found for GaMnN with low Mn concentration and hence, a strong reduction in the intensity of the Mn-related blue band emission around 3.0 eV was observed.

3.5. Electron paramagnetic resonance

Electron paramagnetic resonance (EPR) in the X band was used to study the incorporation and the electronic structure of the manganese ions in GaN. In the X band only the typical spectra of isolated Mn^{2+} were observed. The characteristic EPR spectra of a 1 μm thick $Ga_{0.978}Mn_{0.022}N$ epilayer for the magnetic field directions B parallel and perpendicular to the hexagonal crystal axis c are shown in Figure 6 together with the corresponding stick spectra. The allowed five fine structure lines generated by the electron spin transitions with $\Delta M = \pm 1$ are resolved, each six fold split by the ^{55}Mn hyperfine interaction due to the coupling of the $^6A_1$ ground state of Mn^{2+} to the nuclear spin I=5/2 of the natural isotope ^{55}Mn. No allowed EPR transition within the Mn^{3+} ground state manifold with S=2 could be observed in the X-band with the available magnetic field. The acceptor states and the compensation mechanism are investigated in more detail by PL and absorption spectroscopy as presented above.

Significant strain or deviations from crystalline symmetry can be ruled out according to the observed small line broadening of the outer fine-structure lines by rotation of the magnetic field B in different crystallographic planes. This conclusion is supported by the determined fine-structure parameter $D = -230 \times 10^{-4}$ cm^{-1} which is similar to that obtained for strain-relieved MBE grown GaN:Mn layers [47]. Furthermore, the isotropic g factor and the isotropic hyperfine parameter A are identical with the values found for Mn-doped GaN-films grown by MBE.

The absence of Mn-induced strain was also confirmed by micro-Raman investigations. Raman spectra of GaMnN with different Mn and carrier concentrations are presented in Figure 6. Raman spectra of GaN epilayers grown on sapphire and on silicon are shown for comparison. Most prominent in all these spectra are the E_2 (high) and the A_1 (LO) Raman modes that were detected at 567 cm^{-1} and 734 cm^{-1}, respectively. These values are in good agreement with those measured for relaxed GaN revealing that no additional strain was introduced even though a high concentration of Mn ions (~10^{20} cm^{-3}) was incorporated in the GaN. A high carrier concentration (above 10^{18} cm^{-3}) was ruled out since no broadening of the A_1 (LO) mode and no LLP modes were detected. According to the stronger strain in the case of the Si substrate, the Raman modes of this sample are shifted to lower energies compared with the epilayers on sapphire.

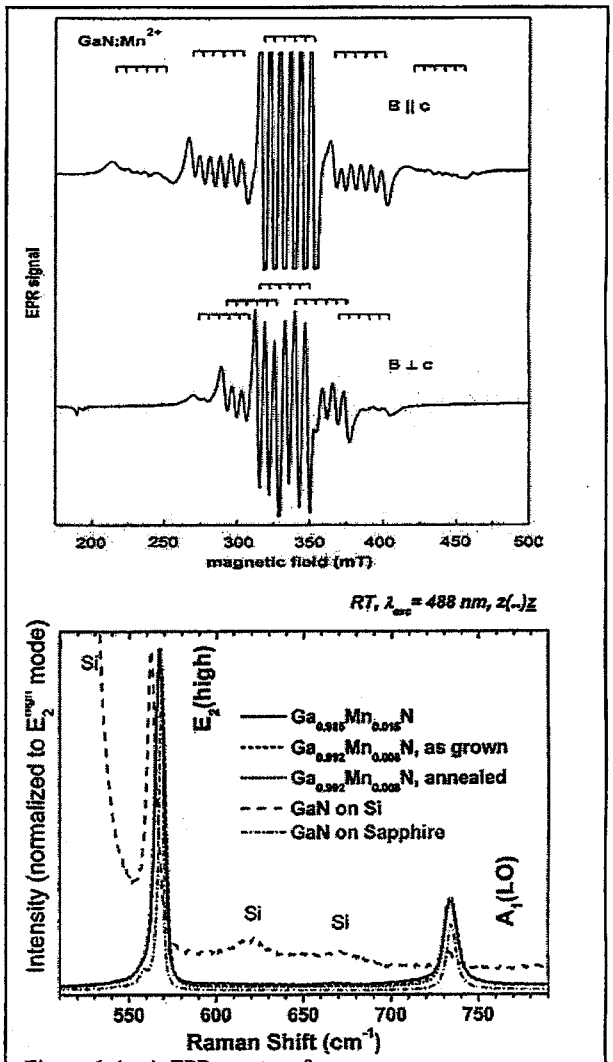

Figure 6 (top) EPR spectra of as-grown $Ga_{0.985}Mn_{0.015}N_{98}Mn_{0.02}N$:Si recorded in magnetic fields parallel and perpendicular to the c-axis at 5K. The presence of Mn^{2+} ions in GaN is unambiguously proven by the hyperfine resonances. (bottom) Raman spectra of MOCVD-grown GaN epilayers with different Mn concentrations and sample preparation. For comparison, GaN epilayers grown on sapphire and on Si substrates are also shown.

3.6. Nanostructure development

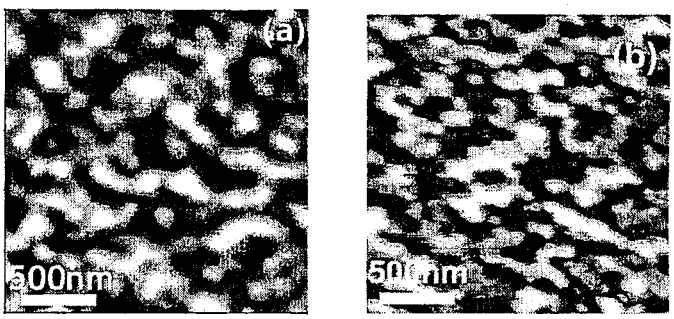

Figure 7: AFM picture of GaN nanostructure (a) and GaMnN nanostructures (b) on AlN. The height of the nanostructures was 40 and 15 nm, respectively.

Initial efforts to incorporate $Ga_{1-x}Mn_xN$ into semiconductor nanostructures via MOCVD have also been attempted. GaN nanostructured islands were grown on AlN via MOCVD using a two-step growth process, which are described in more detail elsewhere [51]. Under optimized process conditions, island aspect ratios of 0.5 and island densities greater than 10^{10} cm^{-2} could be achieved. Mn doping results in nanostructures similar heights but a twofold reduction in island density. These results suggest that Mn introduces a slight surfactant effect counteracting the 3D growth mode. In order to achieve multifunctional nanostructures combining the advantages of quantum dots and diluted magnetic semiconductors (see Figure 7), initial nucleation studies on GaMnN grown on AlN epilayers were performed. Controlling incorporation of transition metal ions in these nanostructures will enable control of their magnetic and optical properties. GaMnN nanostructures were grown by introducing Mn to GaN flows under optimal conditions for the formation of nanostructure. The surface morphology was strongly affected by the presence of Mn atoms, as shown in Figure 7. The AFM characterization revealed that both the island density and the island sizes are altered in comparison to GaN nanostructures. The nanostructures achieved upon Mn doping have lateral dimensions > 100 nm and an average height of 15 nm. The nanostructures' height was reduced and the density decreased by a factor of two in comparison to the nanostructure growth without Mn exposure. These results suggest that Mn introduces a slight surfactant effect counteracting the 3D growth mode. In consequence, stronger anti-surfactant conditions have to be applied to maintain the formation of multifunctional nanostructures. As confirmed in our studies, the anti-surfactant effect introduced by Si holds for this requirement. It might be speculated here that a metallic gallium bi-layer [52, 53] or the island formation in a submonolayer growth mode [54, 55] imply similar effects.

4. Conclusions

High quality $Ga_{1-x}Mn_xN$ has been grown by metalorganic chemical vapor deposition (MOCVD. Almost no change in the structural properties was observed with Mn incorporation at dilute quantities (<2%). Upon annealing, the non-equilibrium material decays through a surface decomposition mechanism resulting in secondary phases; terminating the surface with a GaN capping layer prevented this surface decomposition. The as-grown films did exhibit ferromagnetism with relatively high magnetic moments per Mn atom. This strong ferromagnetism could be destroyed through the introduction of shallow compensating donors, either through high temperature annealing processes or through intentional co-doping of the layers with silicon. This is attributed to a filling of holes in a Mn impurity band, preventing long range ferromagnetic double exchange coupling of the isolated magnetic centers

High concentrations of Mn on Ga site (between 0.3% and 2%) were incorporated in $Ga_{1-x}Mn_xN$ by MOCVD growth. According to the high Mn concentration, the T_2 states of the Mn 3d shell were broadened. This broadening was confirmed by the observation of a respective absorption band around 1.5 eV related to inner ^5D state transitions (T_2 to E) of Mn ions. This absorption scaled with the Mn concentration. In contrast, this band vanished when the concentration of free electrons was increased (e.g., by Si co-doping and by annealing) leading to the compensation of the partially filled T_2 band that equals the transition from the Mn^{3+} to the Mn^{2+} state. In this case, also the saturation magnetization decreased confirming the Fermi-level dependence of the ferromagnetism.

ACKNOWLEGEMENTS

Work at Georgia Tech has been supported by the Grant #F49620-03-1-0294 from the Air Force Office of Scientific Research (T. Steiner) and the National Science Foundation (ECS#0224266, U. Varshney). Support for one author (M.K.) has been provided through a NDSEG fellowship sponsored by the Department of Defense. M.S. was supported by the Feodor-Lynen program of the Alexander von Humboldt-foundation. The authors thank A. M. Payne for secondary ion mass spectroscopy measurements and D. Nicol for annealing some of the samples.

REFERENCES

[1] S. A. Wolf, "Spintonics, Electronics for the Next Millenium," *Journal of Superconductivity*, vol. 13, pp. 195-199, 2000.

[2] S. A. Wolf, D. D. Awschalom, R. A. Buhrman, J. M. Daughton, S. von Molnar, M. L. Roukes, A. Y. Chtchelkanova, and D. Treger, "Spintronics, A Spin-Based Electronics Vision for the Future," *Science*, vol. 294, pp. 1488-1495, 2001.

[3] H. Ohno, F. Matsukura, and Y. Ohno, "Semiconductor Spin Electronics," *JSAP International*, vol. 8, pp. 4-13, 2002.

[4] D. D. Awschalom, M. E. Flatte, and N. Samarth, "Spintronics," *Scientific American*, pp. 67-73, 2002.

[5] H. Ohno, "Molecular beam epitaxy and properties of ferromagnetic III-V semiconductors," *Journal of Crystal Growth*, vol. 251, pp. 285-291, 2003.

[6] T. Dietl, H. Ohno, F. Matsukura, J. Cibert, and D. Ferrand, "Zener Model Description of Ferromagnetism in Zinc-Blende Magnetic Semiconductors," *Science*, vol. 287, pp. 1019-1022, 2000.

[7] L. Kronik, M. Jain, and J. R. Chelikowsky, "Electronic structure and spin polarization of MnxGa1-xN," *Physical Review B*, vol. 66, pp. 041203, 2002.

[8] K. Sato, P. H. Dederichs, H. Katayama-Yoshida, and J. Kudrnovsky, "Magnetic impurities and materials design for semiconductor spintronics," *Physica B*, vol. 340-342, pp. 863–869, 2003.

[9] K. Sato and H. Katayama-Yoshida, "First principles materials design for semiconductor spintronics," *Semiconductor Science & Technology*, vol. 17, pp. 367-76, 2002.

[10] T. Graf, M. Gjukic, M. S. Brandt, M. Stutzmann, and O. Ambacher, "The Mn3+2+ Acceptor level in Group III Nitrides," *Applied Physics Letters*, vol. 81, pp. 5159-5161, 2002.

[11] H. Akai, "Ferromagnetism and its stability in the Diluted Magnetic Semiconductor (In,Mn)As," *Physical Review Letters*, vol. 81, pp. 3002-3005, 1998.

[12] M. Zajac, J. Gosk, M. Kaminska, A. Twardowski, T. Szyszko, and S. Podsiadlo, "Paramagnetism and antiferromagnetic d-d coupling in GaMnN magnetic semiconductor," *Applied Physics Letters*, vol. 79, pp. 2432-2434, 2001.

[13] W. Gebickia, J. Strzeszewski, G. Kamler, T. Szyszko, and S. Podsiadlo, "Raman scattering study of Ga1-xMnxN crystals," *Applied Physics Letters*, vol. 76, pp. 3870-3872, 2000.

[14] T. Szyszko, G. Kamler, B. Strojek, G. Weisbrod, S. Podsiadlo, L. Adamowicz, W. Gebicki, J. Szczytko, A. Twardowski, and K. Sikorski, "Growth of bulk Ga1-xMnxN single crystals," *Journal of Crystal Growth*, vol. 233, pp. 631-638, 2001.

[15] N. Theodoropoulou, A. F. Hebard, M. E. Overberg, C. R. Abernathy, S. J. Pearton, S. N. G. Chu, and R. G. Wilson, "Magnetic and structural properties of Mn-implanted GaN," *Applied Physics Letters*, vol. 78, pp. 3475-3477, 2001.

[16] M. H. Kane, A. Asghar, A. M. Payne, C. R. Vestal, Z. J. Zhang, M. Strassburg, J. Senawirante, N. Dietz, C. J. Summers, and I. T. Ferguson, "Comparison of GaMnN epilayers prepared by ion implantation and metalorganic chemical vapor deposition," *Physica Status Solidi*, vol. C, pp. Submitted, 2004.

[17] K. P. Lee, S. J. Pearton, and M. E. Overberg, "Magnetic Effects of Direct Ion Implantation of Mn and Fe into p-GaN," *Journal of Electronic Materials*, vol. 31, pp. 411-15, 2002.

[18] C. Liu, E. Alves, A. D. Sequeira, N. Franco, M. F. d. Silva, and J. C. Soares, "Fe ion implantation in GaN: Damage, annealing, and lattice site location," *Journal of Applied Physics*, vol. 90, pp. 81-86, 2001.

[19] N. Theodoropoulou, A. F. Hebard, S. N. G. Chu, M. E. Overberg, C. R. Abernathy, S. J. Pearton, and R. G. Wilson, "Use of ion implantation to facilitate the discovery and characterization of ferromagnetic semiconductors," *Journal of Applied Physics*, vol. 91, pp. 7499-7501, 2002.

[20] R. M. Frazier, G. T. Thaler, C. R. Abernathy, S. J. Pearton, M. L. Nakarmi, K. B. Nam, J. Y. Lin, H. X. Jiang, J. Kelly, R. Rairigh, A. F. Hebard, J. M. Zavada, and R. G. Wilson, "Transition metal ion implantation into AlGaN," *Journal of Applied Physics*, vol. 94, pp. 4956-4960, 2003.

[21] Y. Shon, Y. H. Kwon, S. U. Yuldashev, C. S. Park, D. J. Fu, D. Y. Kim, H. S. Kim, and T. W. Kang, "Diluted magnetic semiconductor of p-type GaN epilayers implanted with Mn+ ions," *Journal of Applied Physics*, vol. 93, pp. 1546-1549, 2003.

[22] M. L. Reed, N. A. El-Masry, H. H. Stadelmaier, M. K. Ritums, M. J. Reed, C. A. Parker, J. C. Roberts, and S. M. Bedair, "Room temperature ferromagnetic properties of (Ga, Mn)N," *Applied Physics Letters*, vol. 79, pp. 3473-3475, 2001.

[23] M. E. Overberg, C. R. Abernathy, S. J. Pearton, N. A. Theodoropoulou, K. T. McCarthy, and A. F. Hebard, "Indication of ferromagnetism in molecular-beam-epitaxy-derived N-type GaMnN," *Applied Physics Letters*, vol. 79, pp. 1312-1314, 2001.

[24] S. Kuroda, E. Bellet-Amalric, X. Biquard, J. Cibert, R. Giraud, S. Marcet, and H. Mariette, "Optimization of the growth of GaMnN epilayers using plasma-assisted MBE," *Physica Status Solidi B*, vol. 240, pp. 443-446, 2003.

[25] S. Sonoda, H. Hori, Y. Yamamoto, T. Sasaki, M. Sato, S. Shimizu, K.-i. Suga, and K. Kindo, "Properties of Ferromagnetic Ga1-xMnxN Films Grown by Ammonia-MBE," *Magnetics, IEEE Transactions on*, vol. 38, pp. 2859-2862, 2002.

[26] J. Kim, F. Ren, A. Y. Polyakov, N. B. Smirnov, A. V. Govorkov, N. Y. Pashkova, G. Thaler, M. E. Overberg, C. R. Abernathy, and S. J. Pearton, "Optical Absorption and Temperature-Dependent Resistivity of GaMnN Grown by Molecular Beam Epitaxy," *Electrochemical and Solid-State Letters*, vol. 5, pp. G103-G105, 2002.

[27] S. Dhar, O. Brandt, A. Trampert, L. Daweritz, K. J. Friedland, K. H. Ploog, J. Keller, B. Beschoten, and G. Guntherodt, "Origin of high-temperature ferromagnetism in (Ga,Mn)N layers grown on 4H-SiC(0001) by reactive MBE," *Applied Physics Letters*, vol. 82, pp. 2077-2079, 2003.

[28] K. Ando, H. Saito, and Z. Jin, "Large magneto-optical effect in an oxide diluted magnetic semiconductor Zn1-xCoxO," *Applied Physics Letters*, vol. 78, pp. 2700-2, 2001.

[29] R. K. Singh, S. Y. Wu, H. X. Liu, L. Gu, D. J. Smith, and N. Newman, "The role of Cr substitution on the ferromagnetic properties of Ga[sub 1 - x]Cr[sub x]N," *Applied Physics Letters*, vol. 86, pp. 012504, 2005.

[30] E. A. Berkman, M. J. Reed, F. E. Arkun, N. A. El-Masry, J. M. Zavada, M. O. Luen, M. L. Reed, and S. M. Bedair, "The Effect of Mn Concentration on Curie Temperature and Magnetic Behavior of MOCVD Grown GaMnN Films," *Materials Research Society Proceedings*, vol. 834, pp. J7.3.1, 2005.

[31] H. Ohno, A. Shen, F. Matsukura, A. Oiwa, A. Endo, S. Katsumoto, and Y. Iye, "(Ga,Mn)As: A new diluted magnetic semiconductor based GaAs," *Applied Physics Letters*, vol. 69, pp. 363-365, 1996.

[32] T. Wojtowicz, W. L. Lim, X. Liu, Y. Sasaki, U. Bindley, M. Dobrowolska, J. K. Furdyna, K. M. Yu, and W. Walukiewicz, "Correlation of Mn Lattice Location, Free Hole Concentration, and Curie Temperature in Ferromagnetic GaMnAs," *Journal of Superconductivity*, vol. 16, pp. 41-44, 2003.

[33] J. D. Boeck, R. Oesterholt, H. Bender, A. V. Esch, C. Bruynseraede, C. V. Hoof, and G. Borghs, "Controlled formation of nanoscale MnAs magnetic clusters in GaAs," *Journal of Magnetism and Magnetic Materials*, vol. 156, pp. 148-150, 1996.

[34] J. M. Baik, H. W. Jang, J. K. Kim, and J.-L. Lee, "Effect of microstructural change on magnetic property of Mn-implanted p-type GaN," *Applied Physics Letters*, vol. 82, pp. 583-585, 2003.

[35] G. T. Thaler, R. M. Frazier, J. Stapleton, C. R. Abernathy, S. J. Pearton, J. Kelly, R. Rairigh, A. F. Hebard, and J. M. Zavada, "Properties of GaMnN with and without detectable second phases," *Electrochemical and Solid-State Letters*, vol. 7, pp. G34-G36, 2004.

[36] B. T. Jonker, "Progress Toward Electrical Injection of Spin-Polarized Electrons into Semiconductors," *Proceedings of the IEEE*, vol. 91, pp. 727-740, 2003.

[37] D. Loss and D. P. DiVincenzo, "Quantum computation with quantum dots," *Physical Review A*, vol. 57, pp. 120, 1998.

[38] M. Holub, S. Chakrabarti, S. Fathpour, P. Bhattacharya, Y. Lei, and K. Ghosh, "Mn-doped InAs self-organized diluted magnetic quantum-dot layers with Curie temperatures above 300 K," *Applied Physics Letters*, vol. 85, pp. 973-975, 2004.

[39] A. Wolos, M. Palczewska, M. Zajac, J. Gosk, M. Kaminska, A. Twardowski, M. Bockowski, I. Grzegory, and S. Porowski, "Optical and magnetic properties of Mn in bulk GaN," *Physical Review B (Condensed Matter and Materials Physics)*, vol. 69, pp. 115210, 2004.

[40] R. Y. Korotkov, J. M. Gregie, and B. W. Wessels, "Optical properties of the deep Mn acceptor in GaN:Mn," *Applied Physics Letters*, vol. 80, pp. 1731-1733, 2002.

[41] O. Gelhausen, E. Malguth, M. R. Phillips, E. M. Goldys, M. Strassburg, A. Hoffmann, T. Graf, M. Gjukic, and M. Stutzmann, "Doping-level-dependent optical properties of GaN:Mn," *Applied Physics Letters*, vol. 84, pp. 4514-4516, 2004.

[42] Y. Shon, Y. H. Kwon, S. U. Yuldashev, J. H. Leem, C. S. Park, D. J. Fu, H. J. Kim, T. W. Kang, and X. J. Fan, "Optical and magnetic measurements of p-type GaN epilayers implanted with Mn+ ions," *Applied Physics Letters*, vol. 81, pp. 1845-1847, 2002.

[43] J. Xu, J. Li, R. Zhang, X. Q. Xiu, D. Q. Lu, S. L. Gu, B. Shen, Y. Shi, and Y. D. Zheng, *Materials Research Society Proceedings*, vol. 693, pp. 207, 2002.

[44] A. Y. Polyakov, N. B. Smirnov, A. V. Govorkov, N. Y. Pashkova, J. Kim, F. Ren, M. E. Overberg, G. T. Thaler, C. R. Abernathy, S. J. Pearton, and R. G. Wilson, "Electrical and optical properties of GaN films implanted with Mn and Co," *Journal of Applied Physics*, vol. 92, pp. 3130-3135, 2002.

[45] M. Strassburg, J. Senawirante, C. Hums, N. Dietz, M. H. Kane, A. Asghar, A. M. Payne, I. T. Ferguson, C. J. Summers, U. Haboeck, A. Hoffman, D. Azamat, and W. Gelhoff, "Optical and Structural Investigations on Mn-Ion States in MOCVD-grown Ga1-xMnxN," *MRS Proceedings*, pp. submitted, 2004.

[46] M. H. Kane, A. Asghar, A. M. Payne, C. R. Vestal, M. Strassburg, J. Senawiratne, Z. J. Zhang, N. Dietz, C. R. Summers, and I. T. Ferguson, "Magnetic hysteresis observed in GaMnN grown by Metalorganic Chemical Vapor Deposition," *Semiconductor Science & Technology*, pp. Submitted.

[47] M. Strassburg, M. H. Kane, A. Asghar, Q. Song, Z. J. Zhang, J. Senawiratne, M. Alevli, N. Dietz, C. J. Summers, and I. T. Ferguson, "Examination of the Fermi Level Dependence of Optical and Magnetic Properties in MOCVD-grown GaMnN," *Physical Review B*, pp. Submitted, 2005.

[48] M. H. Kane, A. Asghar, M. Strassburg, Q. Song, A. M. Payne, C. J. Summers, Z. J. Zhang, N. Dietz, and I. T. Ferguson, "Impact of Manganese incorporation on the structural and magnetic properties of MOCVD-grown Ga1-xMnxN," *Materials Research Society Proceedings*, vol. 831, pp. E9.4.1, 2005.

[49] T. Graf, M. Gjukic, M. Hermann, M. S. Brandt, M. Stutzmann, and O. Ambacher, "Spin resonance investigations of Mn2+ in wurtzite GaN and AlN films," *Physical Review B*, vol. 67, pp. 165215, 2003.

[50] J. M. Baik, J.-L. Lee, Y. Shon, and T. W. Kang, "Microstructural, optical, and magnetic properties of Mn-implanted p-type GaN," *Journal of Applied Physics*, vol. 93, pp. 9024-9029, 2003.

[51] S. Gupta, H. Kang, M. Strassburg, A. Asghar, J. Senawirante, N. Dietz, and I. T. Ferguson, "A Nucleation Study of GaN Multifunctional Nanostructures," *Materials Research Society Proceedings*, vol. 831, pp. E12.7.1, 2005.

[52] N. Gogneau, D. Jalabert, E. Monroy, T. Shibata, M. Tanaka, and B. Daudin, "Structure of GaN quantum dots grown under ``modified Stranski--Krastanow" conditions on AlN," *Journal of Applied Physics*, vol. 94, pp. 2254, 2003.

[53] J. Brown, F. Wu, P. M. Petroff, and J. S. Speck, "GaN quantum dot density control by rf-plasma molecular beam epitaxy," *Applied Physics Letters*, vol. 84, pp. 690, 2004.

[54] S. Tanaka, I. Suemune, P. Ramvall, and Y. Aoyagi, "GaN Quantum Structures with Fractional Dimension - From Quantum Well to Quantum Dot," *physica status solidi b*, vol. 216, pp. 431, 1999.

[55] I. L. Krestnikov, N. N. Ledentsov, A. Hoffmann, and D. Bimberg, "Arrays of Two-Dimensional Islands Formed by Submonolayer Insertions: Growth, Properties, Devices," *physica status solidi a*, vol. 183, pp. 207-233, 2001.